Hindawi
International Journal of Polymer Science
Volume 2020, Article ID 6421470, 15 pages
https://doi.org/10.1155/2020/6421470

Research Article

Recycling and Reusing Polyethylene Waste as Antistatic and Electromagnetic Interference Shielding Materials

Mostafizur Rahaman, Ibrahim Abdullah Al Ghufais, Govindasami Periyasami, and Ali Aldalbahi

Department of Chemistry, College of Science, King Saud University, Riyadh 11451, Saudi Arabia

Correspondence should be addressed to Mostafizur Rahaman; mrahaman@ksu.edu.sa and Ali Aldalbahi; aaldalbahi@ksu.edu.sa

Received 22 December 2019; Revised 27 February 2020; Accepted 27 May 2020; Published 13 June 2020

Academic Editor: Anjanapura V. Raghu

The aim of this work is to manage the waste product based on polyethylene (PE) films by recycling and reusing it as antistatic material for electronic packaging and electromagnetic interference (EMI) shielding material for protecting electronic equipment from interference of EM radiation. To achieve this, a conductive carbon black has been mixed with the PE waste at different weight percent values by ultrasonication via a solution mixing process. Mixing time for sonication was determined by ultraviolet-visible (UV-VIS) spectra. A differential scanning calorimetry (DSC) study showed that the low-density polyethylene (LDPE) and linear low-density polyethylene (LLDPE) are immiscible in their blend composition. The tensile properties of PE have reduced substantially after reprocessing. However, the addition of carbon black has improved its strength up to a certain loading. The electrical percolation threshold values, calculated using the classical power law and sigmoidal Boltzmann model, were obtained at 3.5 and 2.8 wt% loading of carbon black, respectively. The conductivity result revealed that 1-2 wt% carbon-loaded composites can be used as antistatic material. The composites, having carbon loading above 4 wt%, can be effective materials for EMI shielding application. The 10 wt% carbon-loaded composite exhibits EMI SE value 33 dB which means there is approximately 99.93% protection of EM radiation at the sample thickness of 1.0 mm. Moreover, FTIR analysis, thermal stability, AC conductivity, dielectric properties, permeability, and current-voltage characteristics are also discussed in detail. There is a substantial increment in thermal stability, and dielectric properties are observed with the addition carbon black loading within the polymer matrix.

1. Introduction

Nowadays, the plastic materials are being increasingly used in our day-to-day life in many fields of applications. These plastic materials, after use, are thrown outside. These are called plastic wastes and are harmful to the environment as most of the plastics are nonbiodegradable in nature. Hence, there is a need for proper management of these waste products to protect our environment. There are many ways to manage these plastic wastes like degradation (thermodegradation, photodegradation, biodegradation, and chemodegradation), land filling, and recycling [1–4]. However, reuse of plastic wastes by recycling is the most important way to protect the environment from these waste products. The drawback associated with this is the deterioration of mechanical properties [5]. Jassim has studied the recycling of polyethylene (PE) waste to produce plastic cement [6]. In this work, the PE waste was mixed at different percentages with Portland cement by replacing sand and lightweight materials were produced, and at a certain percentage of PE, there was improvement in product ductility and workability. There are also many reports of recycling PE-based plastics in the past by different researchers [7–9]. Choudhury et al. studied the recycling of PE/nylon 6-based oil pouches using two different compatibilizers and reported a substantial improvement in the thermal and mechanical properties of the recycled product [7]. Manos and his coworkers reported the recycling of PE waste by converting it into hydrocarbon

fuel using the catalytic cracking method over aluminum pillared clay catalysts [9]. The plastic wastes are also reused in building and road construction purposes, making pavements, power generation, and waste to energy recovery [10–16]. Moreover, the PE wastes, which are used in film packaging application in our daily life, are recycled and again reused for the same packaging purposes. In most cases, these PE wastes are recycled by adding some extra stabilizing additives within and are reused for the same purposes [17]. However, by adding some carbonaceous additives/fillers within, one can recycle these PE wastes and reuse them for some other purposes such as antistatic (electrostatic discharge (ESD)) and electromagnetic interference (EMI) shielding materials.

An antistatic material is a material which is used to reduce static electricity to protect electrostatic sensitive devices by inhibiting triboelectric charging. This type of charge is built up by rubbing or being in contact with another material. The development of static charge can destroy sensitive electronic components, erase magnetic media, and even set off fire or explosion. Hence, the researchers are developing antistatic material to protect the electronic equipment. The antistatic material is made of that material; that is, the material is itself slightly conductive, or the surfaces of the material or the material as a whole is slightly conductive with the addition of external conductive additives. There are some published literatures where the antistatic property of the virgin PE-based composites was discussed [18–20]. Wang and his coworkers have prepared highly antistatic PE/polyaniline-encapsulated graphene nanoplatelet composites by the solution mixing process and reported that at 10 wt% graphene loading into polyaniline nanocomposites, a permanent antistatic material was formed [21].

EMI shielding materials are used to protect the electronic equipment and other communication devices from unwanted EM radiations, which interfere with the device signal and cause the malfunctioning of the instruments [22, 23]. Although mostly metals are used as EMI shielding materials, these suffer from high weight, process difficulty, and lack of flexibility and are prone to oxidation [22]. Hence, recently, polymer-based conductive composites are developed and widely used as EMI shielding materials [24–27]. There is also a report of using neat PE/carbon nanotube (CNT) composites as EMI shielding materials where three types of CNTs are used with different network structures [28]. It has been observed that segregated network-structured composites showed the excellent EMI shielding effectiveness of 46 dB at only 5 wt% CNT loading compared to other structured composites. However, though the virgin PE composites are used as antistatic and EMI shielding materials, studies on the use of recycled PE as both antistatic and EMI shielding materials are really scanty.

Hence, the objective of this research work is to recycle the PE film waste and reuse it as antistatic (ESD) and EMI shielding materials by adding carbon black as a conductive additive within its matrix. The recycled films have been prepared by solvent casting technique. These films can be used for the purpose of electronic packaging and protecting electronic equipment from interference with EM radiation. The DC electrical conductivity and EMI SE of the composites have been investigated to check their suitability as antistatic and shielding materials. In addition, the FTIR analysis and mechanical, thermal, AC electrical, and dielectric properties of the PE/carbon composites have been tested to check the improvement/reduction of properties. Finally, it can be said that through this waste management, the environment can be cleaned and the plastic wastes can be reused for other purposes.

2. Materials, Methods, and Experiments

2.1. Materials. The polyethylene (PE) transparent film was collected from Minigrip, Alpharetta, GA, USA. It is a blend of LDPE (low-density polyethylene) and LLDPE (linear low-density polyethylene) (70/30) with density 0.91 g/cm^3 and M_w1.42 × 10^5 g/mol. Printex XE2 carbon black was supplied by Degussa Canada Limited, Burlington, ON, Canada. The solvent toluene was procured from Winlab Limited, Maidenhead, Berkshire, UK.

2.2. Methods. The recycling of the polymer and its composites was carried out by solution mixing technique [29]. In this typical procedure, 0.4 g PE film waste, after washing several times with detergent and distilled water and drying in an oven at 50°C, was dissolved in 50 ml of toluene using a magnetic stirrer. In a separate beaker, the required quantity of carbon black was dispersed within 50 ml of toluene for 15 min using a magnetic stirrer. The dispersed carbon black was then added to the dissolved PE and sonicated at 90°C up to their optimum time of sonication as determined by UV-VIS spectra. The mixture was then cast into a Petri dish at elevated temperature (70°C) to form a composite film. The process was repeated to make different composites of polyethylene and carbon black given in Table 1. Finally, the film was dried under vacuum at 50°C. The composites' designations are given in Table 1. The measured density of the composites PEC1, PEC2, PEC4, PEC6, PEC8, and PEC10 is 0.918, 0.927, 0.944, 0.960, 0.976, and 0.991, respectively.

2.3. Experiments

2.3.1. UV-VIS Spectra. The sonication was performed at the amplitude 10 and pulse rate 30 sec off-on. The optimum sonication time for the composites was determined using the Spectro UV-VIS (Model UVD-3500) double beam automatic scanning spectrophotometer (Labomed Inc., Los Angeles, CA, USA) within the wavelength range 200-800 nm. For a particular composite, many tests were done after a certain interval of time and stopped when the spectra overlapped each other. The dilution ratio of the test was 1 : 12.

2.3.2. Differential Scanning Calorimetry. Differential scanning calorimetry (DSC, Q1000, TA instruments, New Castle, DE, USA) of the samples was performed within the temperature range 30-300°C at the ramp rate 10°C/min under nitrogen environment. Nitrogen flowed at the rate 50 ml/min. The test was conducted for both the heating and cooling cycles.

Table 1: Formulations of polyethylene (PE)/Printex carbon black composites.

SN	Weight in per hundred polymer (php)	
	PE	Printex carbon black
PE	100	0
PER	100	0
PEC0.25	100	0.25
PEC0.50	100	0.50
PEC1	100	1
PEC2	100	2
PEC4	100	4
PEC6	100	6
PEC8	100	8
PEC10	100	10

2.3.3. Electrical Properties. The DC electrical conductivity of the samples, having high resistance, was measured using a high-resistance meter Agilent 4339B (Agilent Technologies, Santa Clara, CA, USA) coupled with an electrode cell (Agilent 16008B Resistivity Cell, Santa Clara, CA, USA). The conductivity of low-resistance samples was measured using a Keysight 34465A Truevolt 6½ digital multimeter (Keysight Technologies, Santa Rosa, CA, USA) attached with a homemade electrode.

The measurement of current-voltage characteristics was performed using the Keysight 34465A Truevolt 6½ digital multimeter. The voltage was applied as input, and the current was noted down as output. The applied voltage range was 1-10 volts.

The AC electrical properties like AC conductivity, dielectric constant, dielectric loss, and magnetic permeability were measured using the instrument QuadTech 7600 (LCR meter) coupled with a homemade electrode. These properties were measured within the frequency range 10-10^6 Hz.

2.3.4. Tensile Properties. The tensile properties of the samples were measured using a tensile testing instrument Instron (Model 3345, Instron, Norwood, MA, USA) as per ASTM D882. The crosshead speed of the test was 500 mm/min. Five samples were tested for each composition. The thickness of the films was 0.2 ± 0.05 mm.

2.3.5. EMI Shielding Effectiveness. The EMI shielding measurement of the test samples was carried out using the instrument Scalar Network Analyzer (HP 8757C, Hewlett Packard). The test instrument was coupled with a sweep oscillator (HP 8350B, Hewlett Packard). The measurement was performed within the X-band frequency range that means 8–12 GHz taking the sample thickness 1.0 mm. Moreover, to test the effect of sample thickness on EMI SE, the sample thickness up to 6 mm was used.

2.3.6. Scanning Electron Microscopy. The dispersion of carbon black within the PE composites was checked through a scanning electron microscope (SEM, model Supra 40, Carl Zeiss SMT AG, Oberkochen, Germany). The specimens were gold coated before the test using a sputter gold coater (model SC7620, Polaron Brand, Quorum Technologies Ltd., East Sussex, UK).

2.3.7. Thermogravimetric Analysis (TGA). The TGA analysis of the samples were performed using the instrument NETZSCH TG 209 F3 Tarsus (NETZSCH, Selb, Germany) within the temperature range 30-800°C at the heating rate 10°C/min. The testing was carried out under nitrogen environment at the flow rate 20 ml/min.

2.3.8. Fourier Transform Infrared (FTIR) Spectra. The FTIR spectra for the samples were carried out using the instrument FTIR-8400 (SHIMADZU Precision Instruments, Inc., California, USA) within the wavenumber range 400-4000 cm^{-1} at ATR mode.

3. Results and Discussion

3.1. Differential Scanning Calorimetry (DSC). Differential scanning calorimetry (DSC) of the neat PE, recycled PE, and their carbon composites has been carried out to check the miscibility of LDPE and LLDPE in their blend composition. We can identify this from the melting behavior of PE that is from their melting temperature. Keeping this point in our mind, the samples are tested from 25°C to 300°C at the scan rate 10°C/minutes. Figure 1 represents the DSC curves of the abovementioned samples. All the samples show dual peaks in their endothermic curve: one melting peak is observed around 106-112°C and another endothermic melting peak is observed around 121 to 124°C. The melting peak around 106 to 112°C is due to the presence of LDPE and around 121 to 124°C is due to the presence of LLDPE [30]. The appearance of two melting points indicates that the blend is immiscible in nature. The cooling curves represent the crystallization behavior of the neat polymer and its recycled composites. The neat PE, PER, and PEC4 samples show two crystallization peaks: the first one is observed within the temperature range 84-101°C and the second one within the temperature range 101-112°C, indicating separate crystallization identity of LLDPE and LDPE in their blend. The composite PEC8 shows a single crystallization peak. The high loading of carbon black may have suppressed the other peaks observed for the rest of the samples. It is observed that there is no substantial variation of the melting and crystallization temperatures after the addition of carbon black within the polymer matrix.

3.2. FTIR Analysis. The data of FTIR analysis of the selected samples like PE, PER, PEC2, PEC4, PEC6, and PEC8 were recorded and shown in Figure 2. Two strong symmetric and asymmetric stretching vibrational bands are observed at 2918 cm^{-1} and 2849 cm^{-1}, respectively, because of the presence of the methylene group (CH_2) in the backbone of the polymer chain [31, 32]. There is the appearance of medium-to-weak peaks at around 1082 cm^{-1} and 555 cm^{-1} due to C-C stretching and bending vibrations in polyethylene, respectively [31]. A strong peak at 720 cm^{-1} is observed because of rocking vibration of CH_2. A sharp band at 1472 cm^{-1} occurred due to asymmetric deformational

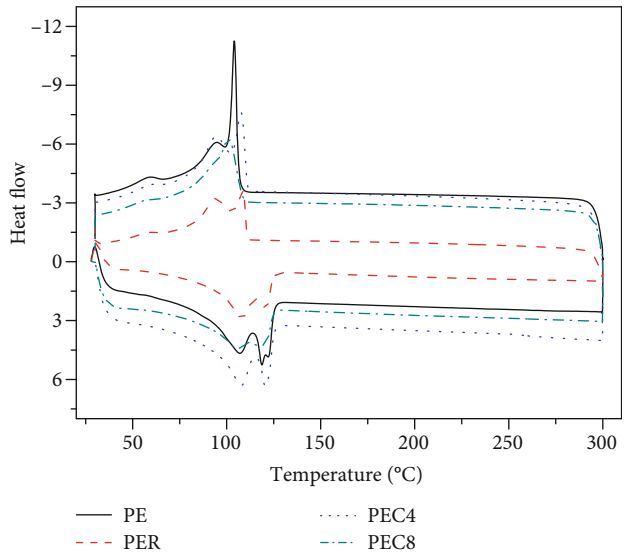

Figure 1: DSC study of PE and its recycled composites.

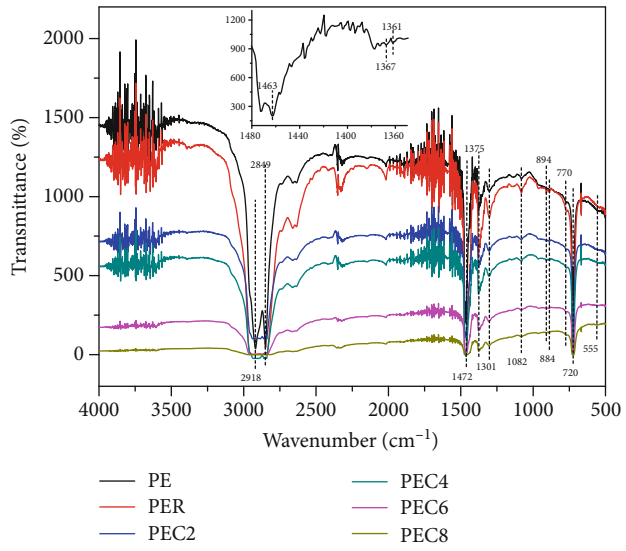

Figure 2: FTIR spectra of PE and its recycled composites.

vibration of the methylene group [31]. A band observed around 1463 cm^{-1} in polyethylene is because of CH_2 scissoring vibration [31, 32]. The vibrational bands around 1367 cm^{-1} and 1137 cm^{-1} are due to CH_2 wagging and twisting, respectively [31, 32]. Methyl deformation and methyl rocking bands are observed around 1375 cm^{-1}, 894 cm^{-1}, and 884 cm^{-1}, respectively, indicating the presence of methyl and butyl type chain branching [32, 33]. The appearance of bands at 770 cm^{-1} indicates the presence of ethyl branches in polyethylene [33]. The band at 1361 cm^{-1} is for methyl wagging deformation and a medium band at 1301 cm^{-1} for methyl twisting deformation. The addition of carbon black has reduced the intensity of bands as is observed from the figure.

3.3. UV-VIS Spectra. A UV-VIS spectral study of the sample PEC4 has been performed to check and find out the mixing time for the composite using an ultrasonicator. The plots based in this study are shown in Figure 3. It is observed from the figure that, with the increase in sonication time, the value of absorbance has increased. This increase in absorbance can be attributed to the increase in the surface area of the carbon black aggregates because of better dispersion within the polymer matrix with respect to increased sonication time [34]. This indicates that the carbon black particles are dispersing more when the sonication time is increased. However, it is observed from the figure that after a certain time (40 min), the curves superimpose on each other, clearly indicating that the full dispersion of carbon black particles within the polymer matric has achieved. Hence, for the present composite system, the mixing time through ultrasonication can be considered 40 min. The UV-VIS absorption of carbonaceous materials is because of the electronic transition between the bonding and antibonding π orbitals: the σ-$\sigma*$ transition occurs within the far UV range 60-100 nm and the π-$\pi*$ transition appears within the range 18-300 nm [34, 35]. Hence, the observed peak around wavelength 280 nm is due to the $\pi \rightarrow \pi*$ transition because of the presence of the conjugated double bond within the molecular structure of carbon [34, 35].

3.4. DC Electrical Conductivity. The electrical conductivity of all composites is shown in Figure 4. It is observed from the figure that the conductivity increases with the increase in the carbon black loading within the polymer matrix. The electrical conductivity of neat PE is 6.78×10^{-18} S/cm, indicating its insulating nature. It can be mentioned herein that the material having electrical conductivity below 10^{-12} S/cm is considered an insulator, within 10^{-12} S/cm to 10^{-8} S/cm an antistatic/ESD (electrostatic discharge) material, and above 10^{-8} S/cm a semiconductor/conductor. These results show that the composite system falls under all three categories. The neat PE, PEC0.25 composite, and PEC0.5 composite are insulating categories; the PEC1 composite and PEC2 composite are antistatic; and the rest of the composites with higher filler loaded carbon are semiconductive/conductive in nature. Hence, the composite systems can be used as an antistatic material and as a semiconductor, depending on the loading of carbon within the polymer matrix. It is observed from the figure that within the insulating range, the increase in electrical conductivity is marginal. The less increment in conductivity in this range is because of the nonforming of any continuous conductive path of carbon particles within the polymer matrix. Hence, the contribution to the electrical conductivity in this insulating range is due to the hopping of charge carriers from one conductive site to another [22, 36]. A substantial increment in conductivity is observed within the antistatic range and antistatic-to-semiconductor transition stage. The increment in conductivity within the antistatic range is because of the increase in the number of conductive sites (due to the increase in filler loading), which reduces the hopping distance and facilitates the electrical conduction [37]. The maximum change in electrical conductivity takes place at the antistatic-semiconductor transition stage, and then, the conductivity increment becomes again marginal. At the transition point, a continuous

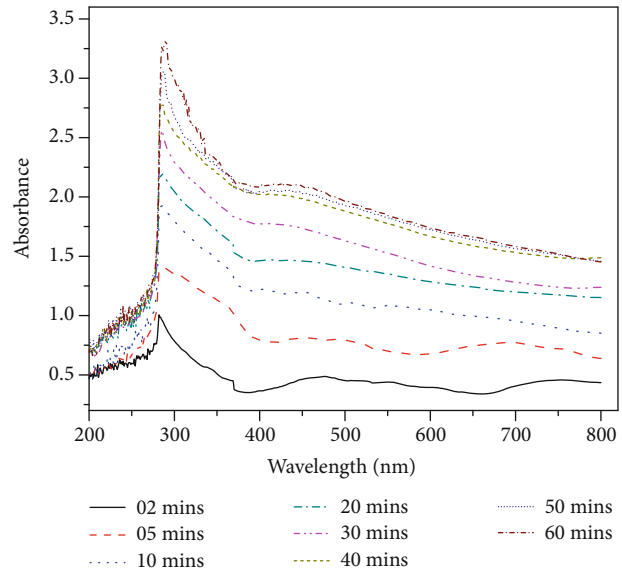

Figure 3: UV-VIS spectral study of the polymer and its recycled composites.

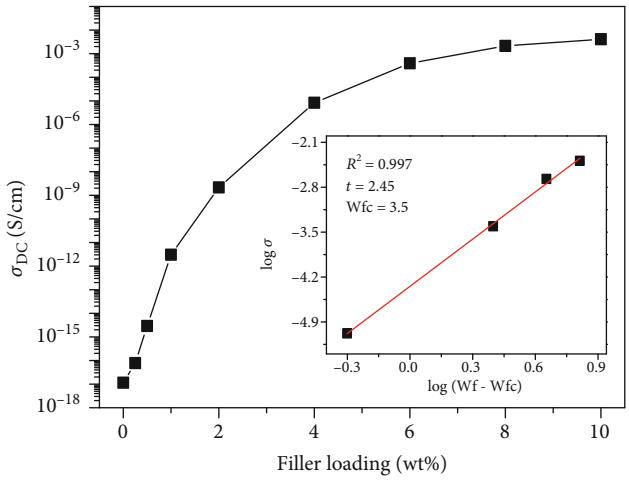

Figure 4: Electrical conductivity of the neat polymer and its recycled composites (inset shows a plot based on classical power law behavior).

network path of conductive sites is formed and accounts for the highest change in conductivity. This transition point is known as the electrical percolation threshold for the composites [22]. Beyond this transition point, because of the addition of more amount of carbon black, the number of continuous conductive path increases and hence results in the marginal increment in conductivity [22]. Figure 5 shows the SEM images at two different resolutions of the neat PE, PEC4 composite, and PEC8 composite, which support the increase in the number of conductive sites with the increase in carbon black loading. Moreover, the presence of many particle-particle contacts facilitates the hopping of charge carriers and their direct flow through the composite system.

The electrical percolation threshold of the composite system has been calculated using the classical power law (Equation (1)) and sigmoidal Boltzmann model (Equation (2)) [38–40]. The equations based on these models are given below:

$$\sigma_c = \sigma_0 (\mathrm{Wf} - \mathrm{Wfc})^t, \quad \text{for Wf} > \mathrm{Wfc}, \tag{1}$$

$$\sigma_c = \sigma_1 + \frac{\sigma_2 - \sigma_1}{1 + e^{(\mathrm{Wf}-\mathrm{Wfc}/\Delta\mathrm{Wf})}}, \tag{2}$$

where σ_c is the conductivity of the composite; σ_0 is a constant quantity that indicates the electrical conductivity of the filler; Wf is the filler loading of the composite; Wfc is the filler loading of the composite at the critical concentration/percolation threshold; t is the critical exponent; σ_1 and σ_2 are the initial and final values of electrical conductivity, respectively; and ΔWf is the fitting parameter/factor. The value of t should be within the range 1.65 to 2.0 for three-dimensional systems [40]. Taking the logarithm of Equation (1), we have the linear equation of the type:

$$\log \sigma_c = \log \sigma_0 + t * \log (\mathrm{Wf} - \mathrm{Wfc}). \tag{3}$$

Hence, plotting log σ_c against log (Wf − Wfc), one can get the value of t from its slope and the value of log σ_0 from its intercept. The plot of the best linear fit, which is obtained at Wfc = 3.5 wt% of carbon black loading where coefficient of correlation $(R^2) = 0.997$, is shown in the inset of Figure 4. The value of the critical exponent t obtained from the slope is 2.45. This value is a little bit higher from the theoretical value mentioned earlier. A similar type of results is also shown in some earlier studies [41, 42]. The value of the percolation threshold, 3.5 wt% of carbon black for our present study, is quite low compared to our previous study, where the same carbon black was used as a filler and melt mixed with the ethylene vinyl acetate (EVA) and acrylonitrile butadiene rubber (NBR) matrices [22]. The percolation threshold value, determined from the sigmoidal Boltzmann model, is 2.8 wt% of carbon black loading. This value of the percolation threshold is less compared to the value determined by the classical power law method. This type of difference has also been observed in our previous study [38].

3.5. AC Electrical Conductivity. The AC conductivity of the neat PE film, PER, and its carbon-filled composite with respect to frequency is shown in Figure 6. It is observed from the figure that the neat PE, PER, and composites possess conductivity below the percolation threshold and show frequency-dependent behavior. However, this frequency-dependent behavior is reduced gradually with the increase of carbon loading in the polymer matrix. The composite, having conductivity around the percolation threshold, shows frequency-independent behavior up to a certain frequency and then becomes frequency-dependent in nature. On the contrary, the composite, having conductivity above the percolation threshold, exhibits totally frequency-independent behavior. The frequency-dependent behavior and frequency-independent behavior of the composites can be explained by considering the electrical conduction mechanism within the polymer matrix. The electrical conduction through a

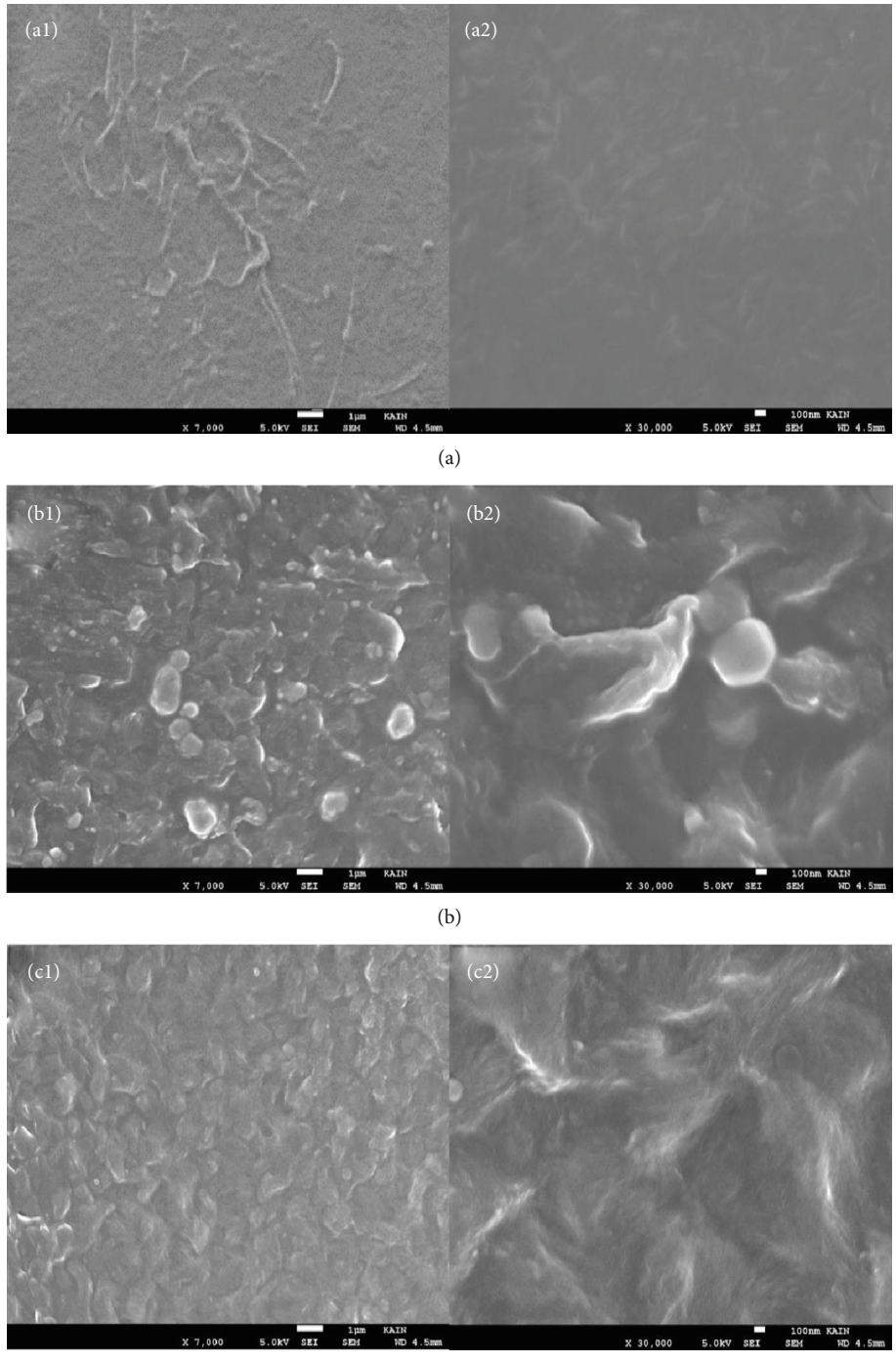

Figure 5: SEM images of (a1) neat PE at low resolution and (a2) neat PE at high resolution, (b1) PEC4 composite at low resolution and (b2) PEC4 composite at high resolution, and (c1) PEC8 composite at low resolution and (c2) PEC8 composite at high resolution.

system takes place by hopping and tunneling of charge carriers [43]. Hopping of charge takes place for mainly nonconducting materials, where the distance among the conductive sites is far enough from each other which means they are not in physical contact with each other. For the neat PE, PER, and composites, possessing conductively below the percolation threshold is having a less number of conductive sites; hence, the electrical conduction through these materials takes place by the hopping process. With the gradual increase in frequency, the charge carriers present in this system get energies, which facilitate the hopping process, and hence, a continuous increase in conductivity is observed. This is why a wide range in variation of conductivity is noticed with the progressive increase in frequency. The observance of frequency-dependent behavior for composites after a certain frequency is because of the activation of some charge carriers

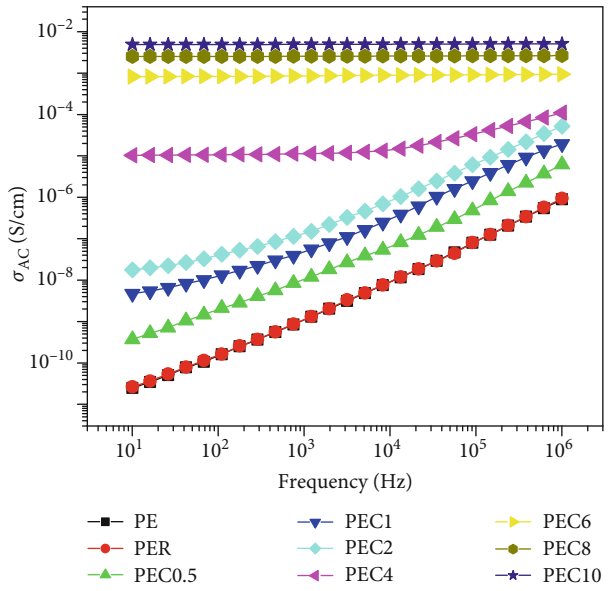

Figure 6: Plots of AC conductivity with respect to frequency for the composite system.

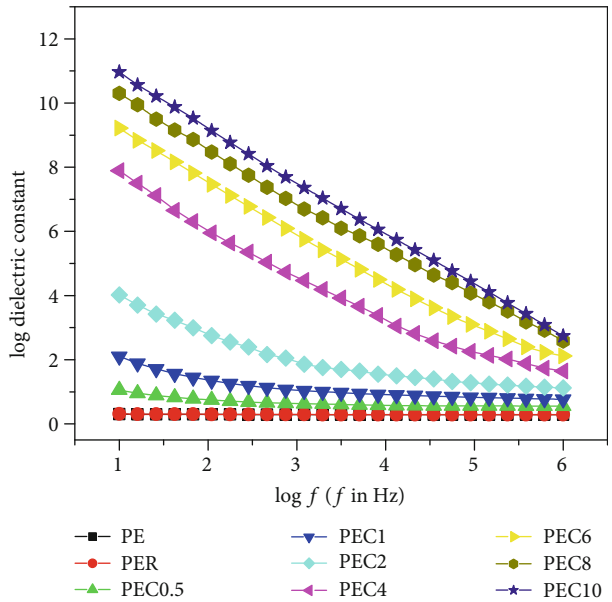

Figure 7: Plots of the dielectric constant with respect to frequency for the composite system.

which were inactive over the previous frequency range. Hence, for the PEC4 composite, the conduction takes place by both tunneling of charge carriers over the 10-10^4 Hz frequency range and hopping of charge carriers over the 10^4-10^6 Hz frequency range. It can be mentioned herein that the tunneling of charge carriers takes place when the conductive sites are in physical contact with each other. For high carbon-loaded composites, that is, the composite having conductivity above the percolation threshold, the number of conductive sites is more and these sites are in contact with each other. As a result, the electrical conduction is mostly governed by the tunneling of charge carriers, and hence, frequency-independent behavior of conductivity is observed.

The AC conductivity at any particular frequency has increased with the increase in carbon black loading within the polymer matrix. The scientific reason behind the increase in conductivity with the increase in carbon black loading has already been discussed in DC Electrical Conductivity.

3.6. Dielectric Constant. The plots of the dielectric constant with respect to the measured frequency range for the neat PE, PER, and composites are presented in Figure 7. It is observed from the figure that the value dielectric constant at any particular frequency increases with the increase in carbon black loading within the polymer matrix. The dielectric property of a material is because of the polarization of dipoles present in the material and alignment of these dipoles towards the applied electric field. For polymer-based composites, two types of polarizations, namely, electronic polarization and interface polarization, occur within the system when the electric field is applied. The carbon particles, present in the system, can be considered the dipoles. The addition of carbon thus increases the number of such dipoles within the composite system. These dipoles create interface polarization at the polymer-filler and filler-filler interfaces, and hence, the dielectric constant value increases with the addition of carbon black loading within the polymer matrix [44]. It is observed from the figure that the increment of the dielectric constant at the lowest frequency is at the order of 10^{11} for the PEC10 composite compared to neat PE. Hence, the result indicates that these composites can be used as a supercapacitor.

The figure also shows that the dielectric constant value decreases with the increase in frequency of the electric field. The magnitude of this decrement is high for higher carbon-loaded composites. Actually, the dipoles present in the system need a certain time to be properly aligned with the direction of the electric field. With the increase in frequency, the dipoles do not get sufficient time for their proper alignment and hence result in the decrease of the dielectric constant value.

3.7. Dielectric Loss. The dielectric loss of the neat PE, PER, and composites is presented in Figure 8. Like the dielectric constant, the dielectric loss value also increases with the increase in carbon black loading within the polymer matrix considering its value at any frequency. The dielectric loss is expressed as the multiplication of the dielectric constant and dissipation factor. Hence, it is the value of the dissipation factor, which governs the value of dielectric loss. The dielectric loss value for the neat PE, PER, and PEC0.5 composite is less compared to their dielectric constant value. This clearly indicates that for these materials, the dissipation of energy is less compared to storage energy (dissipation factor is less than unity). This energy is dissipated because of the movement of dipoles towards the applied electric field [45]. However, the composites, having high filler loading, exhibit a higher value of dielectric loss compared to its dielectric constant value. This indicates that the energy loss is more compared to storage energy for these composites. Hence, these composites are called lossy dielectric. The higher value

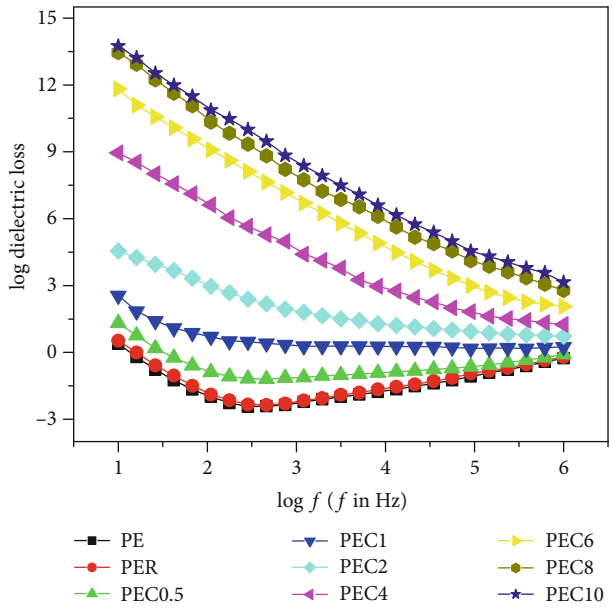

Figure 8: Plots of dielectric loss with respect to frequency for the composite system.

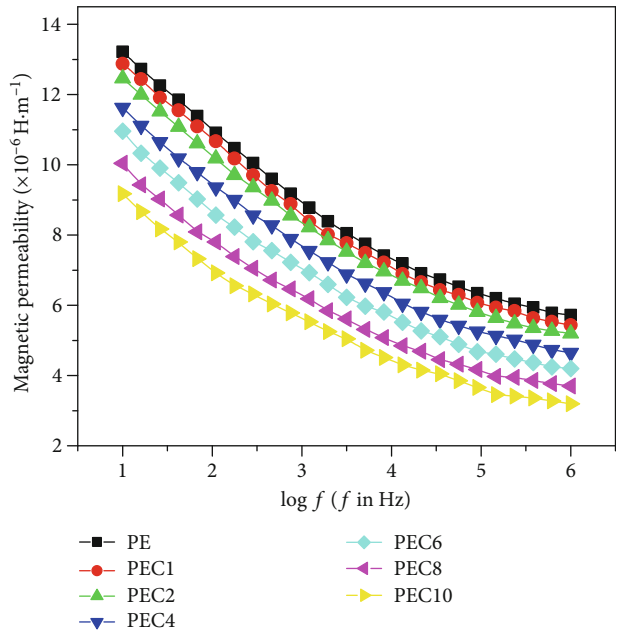

Figure 9: Plots of magnetic permeability with respect to frequency for the selected composite system.

of loss for higher carbon-loaded composites is because of the presence of more number of dipoles, which loses more energy for their movement towards the applied electric field.

The dielectric loss value also decreases like the dielectric constant value when frequency of the electric field is increased. However, the trend is the same except for PE and PER. In this case, initially, the dielectric loss reduces up to a certain frequency and then increases. This increase in dielectric loss over the higher frequency region may be because of the loss due to orientation of more dipoles which were inactive at lower frequencies.

3.8. Permeability. The magnetic permeability of the PE, PER, and composites is shown in Figure 9, which shows that the value of permeability decreases gradually with the addition of increasing carbon black loading within the polymer matrix when we consider the value at any frequency. It is a well-known fact that the value of relative magnetic permeability for diamagnetic materials is always less than unity, whereas for the ferromagnetic and paramagnetic materials, it is higher than unity. It is multifold higher than unity for ferromagnetic materials and slightly higher for paramagnetic materials. The ferromagnetic and paramagnetic materials are attracted towards the magnetic field, whereas the diamagnetic materials repel the magnetic field [46]. Herein, the added filler, carbon black, is a diamagnetic material in nature, and hence, its addition within the polymer matrix results in the gradual decrease in its permeability value.

It is also observed from the figure that the value of permeability decreases with the increase in frequency. This decrement permeability is because of the loss of Eddy current, which decreases with the increase in frequency [47]. A similar type of observation has also been reported elsewhere [47, 48].

3.9. Tensile Property. The tensile stress-strain behavior of the neat PE film and its composites is presented in Figure 10. The samples exhibit the cold drawing process. As expected, the neat PE film shows yield stress at low elongation, necking formation, and strain hardening at high elongation. At the beginning, elastic deformation of all samples is observed, where there is almost uniform reduction in the cross-sectional area with the increase in sample length. At the yield point, the transition of elastic deformation to plastic deformation takes place. Initially, the yield is formed due to the reorientation and destruction of lamellae as yielding is dependent on lamellar thickness [49]. After the yield point, there is a sudden reduction of the cross-sectional area of the sample at a particular position that is the formation of the neck, which propagates along the gauge length of the sample. As a result, the stress falls down and remains almost constant up to a certain strain. Further straining of the sample results in the increase in stress because of strain hardening of the sample resulting from the stress-induced crystallization [49]. Finally, the sample starts to break, where the fall of stress is observed. On the contrary, the PER, PEC0.5, PEC1, PEC2, and PEC4 show yield stress and necking phenomena but no strain hardening is observed. Moreover, the composites, having higher black loading, show no yield point, necking phenomena, or strain hardening. It is interesting to see herein that the nature of plots also changes when the addition of carbon black amount increases.

The tensile parameters like tensile strength, tensile modulus, and tensile strain are extracted from the figure and shown in Table 2. It is seen from the table that there is a drastic decrement in tensile parameters for the recycled unfilled PE compared to the neat PE. During reprocessing through sonication, the extensive shearing force is exerted on the polymer. This results in the degradation of the polymer by

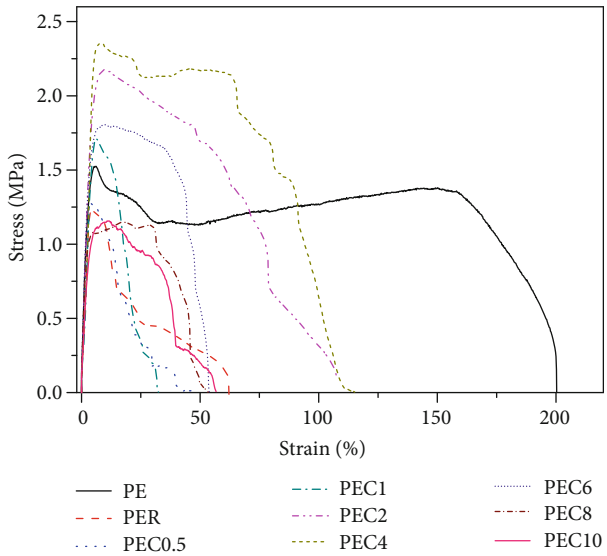

Figure 10: Stress-strain behavior of the polymer and its recycled composites.

Table 2: Tensile parameters like tensile strength, modulus, and strain (%).

Samples	Tensile strength (MPa)	Tensile Modulus (MPa)	Tensile strain (%)
PE	1.52 ± 0.14	58.6 ± 3.4	201 ± 23
PER	1.23 ± 0.10	39.7 ± 2.8	062 ± 16
PEC0.5	1.28 ± 0.11	43.8 ± 3.0	048 ± 13
PEC1	1.71 ± 0.13	45.9 ± 3.1	032 ± 11
PEC2	2.18 ± 0.16	51.5 ± 2.9	108 ± 18
PEC4	2.36 ± 0.18	66.8 ± 3.8	115 ± 19
PEC6	1.81 ± 0.13	52.3 ± 3.3	054 ± 12
PEC8	1.15 ± 0.09	42.4 ± 2.7	053 ± 10
PEC10	1.16 ± 0.12	32.2 ± 2.6	056 ± 08

molecular chain scission. Hence, the polymer chain length is reduced, which results in the decrease polymer molecular weight. As a result, all tensile parameters are reduced after recycling the polymer [50]. The addition of carbon black has increased the tensile strength and modulus up to the loading of 4 wt% which then declined. The initial increment in strength and modulus is due to the reinforcing dominant nature of the interfacial polymer-filler interaction, which declines at higher filler loading because of the dominant nature of the nonreinforcing filler-filler interaction [51, 52]. The elongation at the break value of the recycled polymer and its composites is low compared to neat polymer. This can be attributed to the breakage of the polymer chain due to the shear rate during the mixing process and reduction in chain mobility because of the polymer-filler interaction [51, 53]. It is seen from the table that though the mechanical properties of the recycled and some composites are reduced, the composites still possess sufficient strength to be usable for different purposes.

3.10. Thermogravimetric Analysis (TGA). The thermal stability of the neat PE, PER, and composites is presented in Figure 11, where Figure 11(a) shows the wt% loss against temperature and Figure 11(b) shows its derivation curve, which represent the maximum degradation temperature of the composites. It is observed from both figures that the neat PE, PER, and composites exhibit one-stage degradation behavior. This single-stage degradation of the samples is because of the breakage of the polymer backbone chain. The extracted parameters from both figures are shown in Table 3, where the onset degradation temperature, maximum degradation temperature, and percent mass residue are reported. It is observed from both the figure and the table that the onset and maximum degradation temperatures for PER have decreased by 7.6°C and 7.7°C, respectively, compared to neat PE. This can be attributed to the structural change of PER because of reprocessing, where there may be breakage of the polymer chain due to the shearing force during the mixing process. But the thermal stability of the polymer has increased because of the addition of carbon black within its matrix. The thermal stability means the onset and maximum degradation temperatures of the PEC8 composite have increased by 24.4°C and 17.1°C, respectively, compared to PER. Actually, the undoped polymer is a bad conductor of heat energy. Hence, with the increase in temperature, the absorbed heat by the polymer is localized, and hence, its degradation occurs. But when carbon black is added with the polymer, it absorbs some heat energy and helps in heat transfer from the polymer to the carbon. As a result, the thermal stability of the polymer has increased [54]. The thermal stability of the PEC10 composite has reduced a little bit compared to the PEC8 composite. This can be attributed to the lack of interaction between the polymer and the carbon for the PEC10 composite, which adversely affects the heat transfer process. It is also observed from both the figures and the table that the % mass residue is increased with the addition of carbon black in the polymer matrix. The highest mass residue for the PEC10 composite is 3.78% at the reported temperature 600°C.

3.11. EMI Shielding Effectiveness. The theory behind the EMI shielding effectiveness is illustrated within the supplementary section. Figures 12(a) and 12(b) represent the EMI shielding effectiveness with respect to frequency and filler loading, respectively. It is observed from the figure that the addition of carbon black within the polymer matrix increases the EMI shielding effectiveness of the composites. The addition of carbon black within the polymer matrix acts as a conductive mesh [22]. It has been mentioned in Supplementary Materials (available here) that the EMI SE of a material is due to the reflection of radiation from the surface of the material, absorption of radiation inside the material, and multiple reflection of radiation within the material. The EMI SE for polymer-based composites is mostly governed by the absorption of radiation within the polymer composite [22, 38]. This absorbed radiation is dissipated as heat energy

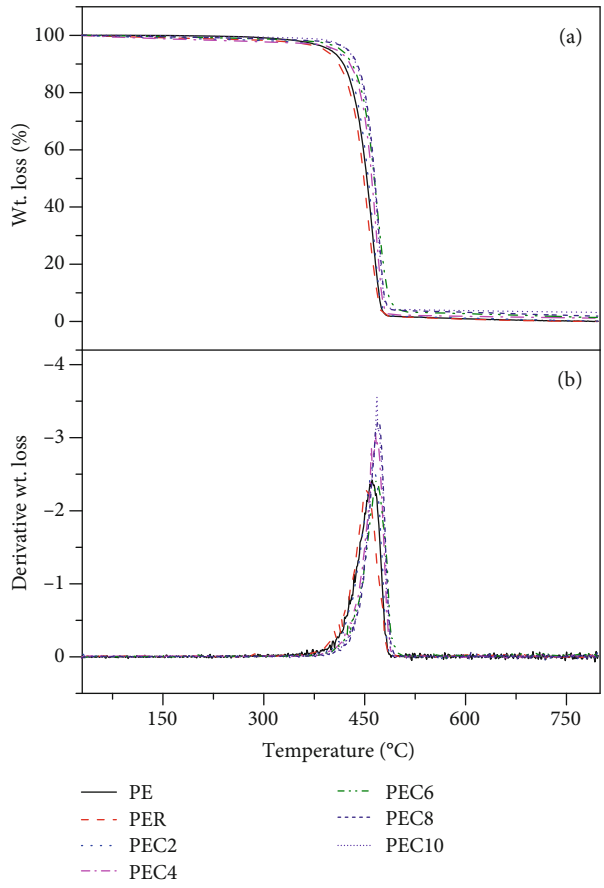

Figure 11: (a) Percent and (b) derivative weight loss of the polymer and composites.

Table 3: Onset degradation temperature, maximum degradation temperature, and % residue at 600°C as extracted from TGA curves.

SN	Onset degradation temperature (°C)	Maximum degradation temperature (°C)	% residue at 600°C
PE	397.8	461.2	0.89
PER	390.2	453.5	0.77
PEC2	404.4	461.9	1.14
PEC4	406.9	466.3	1.79
PEC6	414.4	467.0	2.69
PEC8	424.6	470.6	3.21
PEC10	423.4	468.3	3.78

after the EMI shielding process. It has been mentioned earlier that the added black acts as a conductive mesh within the polymer matrix. The EM radiation interferes with these conductive meshes and gets absorbed. With the increase in black loading, the number of such type of conductive mesh increases; as a result, the absorption of radiation is also increased and thereby leads to the increasing value of EMI SE with the increase in carbon black loading [55].

A comparison of the incremental trend between EMI SE and conductivity is shown in Figure 12(b). It is observed that the incremental trend of both curves is quite different. The conductivity curve is almost exponential in nature, whereas the EMI SE curve is almost linear. The increment in log conductivity before and after the percolation threshold is 10.8 S/cm and 3.6 S/cm, respectively. Hence, before percolation, the increase in conductivity is 200% more compared to the increase in conductivity after the percolation threshold. On the contrary, the increase in EMI SE before and after the percolation threshold is 14.3 dB and 17.85 dB, respectively, indicating that the EMI SE increment before the percolation threshold is 19.9% less compared to the EMI SE increment after the percolation threshold. This difference in the behavior of conductivity and the EMI SE increment can be explained by considering the mechanism of electrical conduction and radiation absorption. It has been mentioned earlier that before the percolation threshold, the electrical conduction is governed mostly by the hopping of charge carriers and at the percolation threshold, the flow of charge carriers takes place through the formed continuous conductive network of carbons. As a result, the increment in electrical conductivity is high enough in this region. After the percolation threshold, more continuous conductive networks are formed, and thereby, the increment in conductivity is marginally less. On the contrary, the increment in EMI SE is dependent on the number and size of conductive meshes present in the composite system. The large number and less sized conductive meshes are more favorable for the absorption of EM radiation and account for the high value of EMI SE. Before the percolation threshold, the number of conductive mesh is less and its size is high; hence, the less increment in EMI SE is observed. But with the increase in carbon black loading beyond the percolation threshold, the number of such type of conductive mesh is increased and its mesh size is decreased. As a consequence, the more increment is observed in EMI SE after the percolation threshold.

It is observed from Figure 12(b) that the composites, having carbon black loading above 4 wt%, exhibit EMI SE value more than 20 dB at the measured thickness. For 10 wt% loaded composite, the EMI SE value is 33 dB. EMI SE values equal to 20 dB and 30 dB indicate 99% and 99.9% protection of EM radiation, respectively. A material, having EMI SE value more than 20 dB, is considered an effective material to be used for shielding radiation. Hence, the higher black-loaded composites can be effectively used for EMI shielding purposes. However, the low carbon black-loaded composites can also be made effective for EMI shielding by increasing their thickness. It is observed from Figure 12(c) that the EMI SE value for the composites increases with the increase in sample thickness. The PEC4 composite, whose EMI SE was below 20 dB at 1.0 mm thickness, now reached above 20 dB at 2.0 mm sample thickness and shows a value approximately 30 dB at 6.0 mm sample thickness. Though the EMI SE of low loaded composites has increased after increasing thickness, the value shows below 20 dB within the measured thickness range. The increase in EMI SE with the increase in thickness is because of the increase in the number of conductive mesh of carbon black in the direction/path of EM radiation [42, 56]. It is also observed that the rate of increase in EMI SE is increasing when we proceed from PE to higher loaded composites. This means that higher conductivity composites exhibit higher rates of increase in EMI SE.

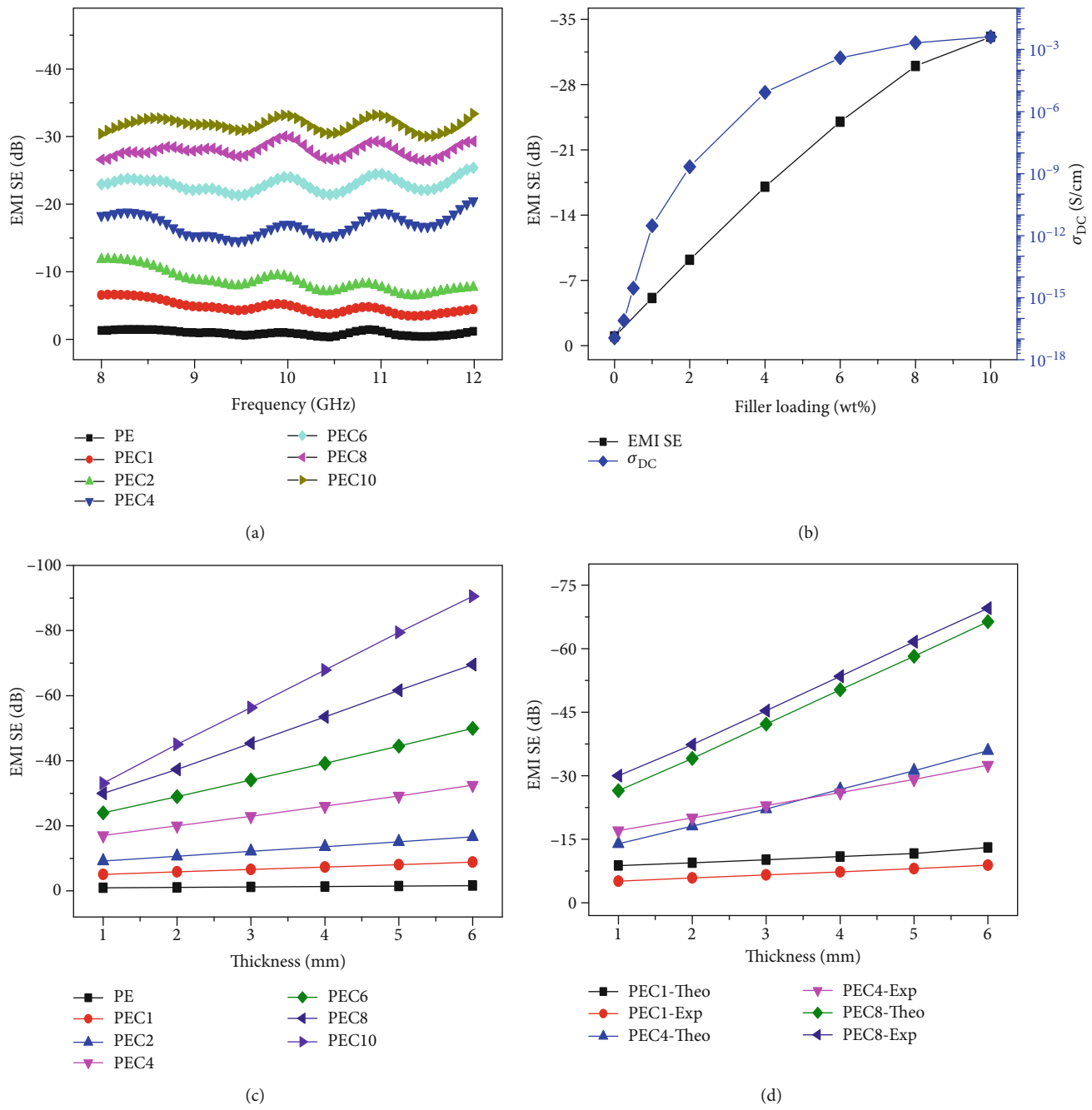

Figure 12: (a) Variation of EMI SE with respect to frequency, (b) comparison of the variation trend of EMI SE and conductivity with respect to filler loading, (c) variation of EMI SE with respect to sample thickness, and (d) theoretical and experimental EMI SE with respect to sample thickness.

The increase in EMI SE with respect to thickness can be calculated theoretically for a single-layer composite and be compared with its experimental value. The equation based on theoretical EMI SE can be given as follows [57]:

$$\text{EMI SE (dB)} = 20 \log\left(1 + \frac{1}{2}\sigma d Z_0\right), \quad (4)$$

where σ is the conductivity; d is thickness of the sample; and Z_0 is the free-space wave impedance, 377 Ω. The theoretical EMI SE values have been calculated for the PEC1, PEC4, and PEC8 composites and compared with their experimental counterparts as shown in Figure 12(d). It is interesting to see from the figure that the theoretical EMI SE shows a high value, cross-over value, and low value for the PEC1, PEC4, and PEC8 composites, respectively, compared to their experimental value over the entire thickness range. These phenomena can be explained by considering the rate of increase in conductivity and EMI SE before and after the percolation threshold. It has been mentioned earlier that the rate of increase in conductivity is high before the percolation

threshold compared to the increase in conductivity after the percolation threshold. As conductivity plays an important role in calculating the theoretical EMI SE as per Equation (4), hence, the contribution of conductivity to calculate EMI SE will be more pronounced for low filler loading composite compared to the composites having filler loading beyond the percolation threshold. Hence, the theoretically calculated EMI SE value for the PEC1 composite is high and for the PEC8 composite is low compared to their experimentally observed values.

The EMI shielding effective values of our PEC10 composite and some other composites, having 10 wt% filler loading, are taken from the published literature and presented in Table 4. A careful observation of this table reveals that the shielding performance of our composite is better compared to other composites except for the GNS/PEDOT:PSS composite one. The higher value of the GNS/PEDOT:PSS composite may be due to the synergistic effect of GNP/PEDOT because of their good combination.

If we compare the tensile result with the EMI shielding value, then it is revealed that the PEC4 composite exhibits the highest tensile strength but poor shielding effectiveness. This can be attributed to the fact that the value tensile strength depends on the dispersion of the filler within the polymer matrix and polymer-filler interaction, whereas the value of EMI shielding effectiveness is governed by the number of conductive mesh within the polymer matrix. With the increase in carbon black loading beyond 4.0 wt%, the polymer-filler interaction is reduced but the number of conductive mesh is increased. This is why though the tensile strength value is high, the EMI shielding effectiveness is less compared to higher carbon-filled composites.

As the material absorbs radiation and this radiant energy is dissipated as heat energy, hence, there will be an increase in temperature of the material. We have tested three composites PEC2, PEC6, and PEC10 to check how much the temperature is increasing after passing radiation for 120 seconds. The temperature increment is 0.4, 0.9, and 1.3°C for the PEC2, PEC6, and PEC10 composites, respectively, indicating that with the increase in carbon loading, the temperature increment also increases.

3.12. Current-Voltage Characteristics. The current-voltage (I-V) characteristics of composites, having electrical conductivity above the percolation threshold, are presented in Figure 13. The plots exhibit that with the increase in voltage, the current also increases, but this increment is a little bit exponential in nature. Hence, the I-V relationship is nonlinear and shows nonohmic behavior. It has been mentioned earlier that the electrical conduction takes place through the composite system by the hopping and tunneling processes. Hopping phenomena happened when the distance between the charge carriers are close enough, that is, approximately 10 Å. In case of tunneling, the charge carriers are in physical contact with each other. This happens with these composites because their conductivity is above the percolation threshold. Hence, there is existence of contact resistance in case of tunneling conduction, which results in the nonlinearity of I-V characteristics [65].

Table 4: EMI SE of the PEC10 composite and some other composites reported in the literature.

Composites	Filler loading (wt%)	Thickness (mm)	EMI SE (dB)	Ref.
CB/PE	10.0	1.0	33.1	Present
CB/PE	10.0	2.0	45.0	Present
CB/PE	10.0	3.0	56.2	Present
CNT/PE	10.0	3.0	35.0	[58]
CNT/PE	10.0	1.65	22.4	[59]
CNT/PP	10.0	2.8	25.0	[60]
CNT/PU	10.0	1.5	29.0	[61]
CNT/PMMA	10.0	2.1	40.0	[62]
GNS/PS	10.0	2.8	18.0	[63]
GNS/PEDOT:PSS	10.0	0.8	46.0	[64]

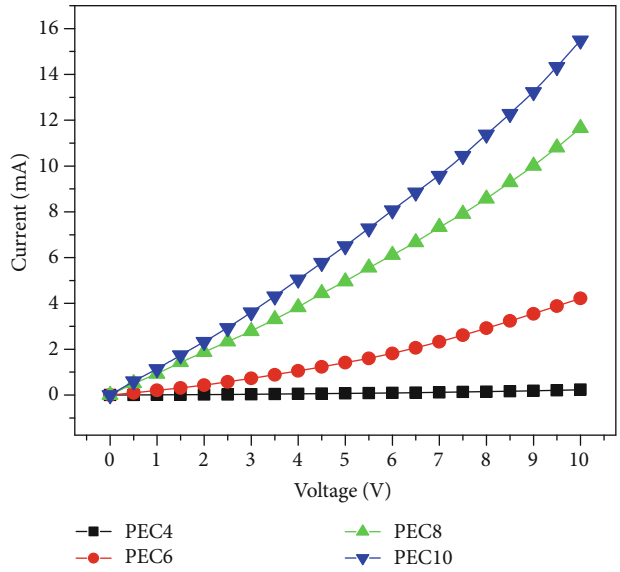

Figure 13: Current-voltage characteristics of selected composites.

4. Conclusions

The results show that there is an approximate variation of electrical conductivity in the order of 10^{14}, which is covering insulating (10^{17}-10^{12} S/cm), antistatic (10^{12}-10^{8} S/cm), and semiconducting ranges (10^{8}-10^{3} S/cm) after 10 wt% addition of carbon black. The electrical percolation threshold values, determined by two different methods, the classical power law and sigmoidal Boltzmann model, were 3.5 and 2.8 wt% of carbon black, respectively. This indicates that the electrical percolation threshold value is dependent on the methods of its determination. The increase in carbon black amount within the PE matrix leads to a peculiar nature/trend of stress-strain plots, which is generally not observed for the virgin PE- and carbon black-based composites. It is seen that though the mechanical properties for recycled and some higher loaded composites have reduced, the composites still possess sufficient strength to be usable for different purposes. Thermal stability has increased by 17.1°C after the addition

of 8 wt% carbon black. There is 10^{11} order increment of the dielectric permittivity value. Approximately 99.93% protection of EM radiation has been achieved for the PEC10 composite at the sample thickness 1.0 mm. This result is superior compared to many studies based on a similar type of composites. The variation of conductivity and EMI SE do not follow the same trend, and this is in accordance with our earlier investigation. It is observed that by increasing sample thickness of low loaded composites, these can be made suitable for use as shielding materials. It is revealed that the experimental value of EMI SE with respect to sample thickness is not in good agreement with its theoretical value. Finally, it can be concluded that the PE waste can be reused as supercapacitors and insulating, antistatic, semiconducting, and radiation shielding materials after its modification by adding suitable additives, and in this way, the plastic wastes can be minimized.

Data Availability

The data used to support the findings of this study are included within this manuscript and supplementary information file.

Conflicts of Interest

There is no competing financial interest among the authors.

Acknowledgments

The authors extend their appreciation to the Deanship of Scientific Research at King Saud University for funding this work through the research group (RG 1438-038).

Supplementary Materials

The EMI shielding theory has been mentioned within the supplementary information section. It expresses how to calculate the EMI shielding effectiveness and its relationship with absorption loss, multiple reflection loss inside the material, and loss due to reflection from the outer surface. A mathematical relation of absorption and reflection loss with conductivity applicable to both the near and far field regions and to both the electric and magnetic fields is also given. *(Supplementary Materials)*

References

[1] A. A. Shah, F. Hasan, A. Hameed, and S. Ahmed, "Biological degradation of plastics: a comprehensive review," *Biotechnology Advances*, vol. 26, no. 3, pp. 246–265, 2008.

[2] J. Siddiqui and G. Pandey, "A review of plastic waste management strategies," *International Research Journal of Environmental*, vol. 2, no. 12, pp. 84–88, 2013.

[3] J. Hopewell, R. Dvorak, and E. Kosior, "Plastics recycling: challenges and opportunities," *Philosophical Transactions of the Royal Society B: Biological Sciences*, vol. 364, no. 1526, pp. 2115–2126, 2009.

[4] S. M. Al-Salem, P. Lettieri, and J. Baeyens, "Recycling and recovery routes of plastic solid waste (PSW): a review," *Waste Management*, vol. 29, no. 10, pp. 2625–2643, 2009.

[5] R. Francis, *Recycling of Polymers: Methods, Characterization and Applications*, John Wiley & Sons, 2016.

[6] A. K. Jassim, "Recycling of polyethylene waste to produce plastic cement," *Procedia Manufacturing*, vol. 8, pp. 635–642, 2017.

[7] A. Choudhury, M. Mukherjee, and B. Adhikari, *Recycling of polyethylene/nylon 6 based waste oil pouches using compatibilizer*, CSIR, 2006.

[8] J. Aguado, D. P. Serrano, G. San Miguel, M. C. Castro, and S. Madrid, "Feedstock recycling of polyethylene in a two-step thermo-catalytic reaction system," *Journal of Analytical and Applied Pyrolysis*, vol. 79, no. 1-2, pp. 415–423, 2007.

[9] G. Manos, I. Y. Yusof, N. H. Gangas, and N. Papayannakos, "Tertiary recycling of polyethylene to hydrocarbon fuel by catalytic cracking over aluminum pillared clays," *Energy & Fuels*, vol. 16, no. 2, pp. 485–489, 2002.

[10] W. Y. Tam Vivian, "Rate of reusable and recyclable waste in construction," *Open Waste Management Journal*, vol. 4, no. 1, pp. 28–32, 2011.

[11] M. A. Kamaruddin, M. M. A. Abdullah, M. H. Zawawi, and M. R. R. A. Zainol, "Potential use of plastic waste as construction materials: recent progress and future prospect," *IOP Conference Series: Materials Science and Engineering*, vol. 267, article 012011, 2017.

[12] K. S. Kumar and K. Baskar, "Recycling of E-plastic waste as a construction material in developing countries," *Journal of Material Cycles and Waste Management*, vol. 17, no. 4, pp. 718–724, 2015.

[13] J. K. Appiah, V. N. Berko-Boateng, and T. A. Tagbor, "Use of waste plastic materials for road construction in Ghana," *Case studies in construction materials*, vol. 6, pp. 1–7, 2017.

[14] M. A. J. Chavan, "Use of plastic waste in flexible pavements," *International Journal of Application or Innovation in Engineering and Management*, vol. 2, no. 4, pp. 540–552, 2013.

[15] A. Khan, K. Nawaz, M. Usama, and Z. Ashraf, "Feasibility study of municipal plastic waste for power generation in Lahore City, Pakistan," *Journal of Chemical Engineering & Process Technology*, vol. 6, p. 229, 2015.

[16] J. A. F. Albanese and M. P. Ruiz, "Gasification of plastic waste as waste-to-energy or waste-to-syngas recovery route," in *Solid Waste as a Renewable Resource*, pp. 267–290, Apple Academic Press, 2015.

[17] C. N. Kartalis, C. D. Papaspyrides, and R. Pfaendner, "Recycling of post-used PE packaging film using the restabilization technique," *Polymer Degradation and Stability*, vol. 70, no. 2, pp. 189–197, 2000.

[18] M. Omastová, S. Kosina, J. Pionteck, A. Janke, and J. Pavlinec, "Electrical properties and stability of polypyrrole containing conducting polymer composites," *Synthetic Metals*, vol. 81, no. 1, pp. 49–57, 1996.

[19] W. Mhike and W. W. Focke, "Surface resistivity and mechanical properties of rotationally molded polyethylene/graphite composites," *Journal of Vinyl and Additive Technology*, vol. 19, no. 4, pp. 258–270, 2013.

[20] J. C. Costa, M. Oliveira, A. V. Machado, S. Lanceros-Méndez, and G. Botelho, "Effect of antistatic additives on mechanical and electrical properties of polyethylene foams," *Journal of Applied Polymer Science*, vol. 112, no. 3, pp. 1595–1600, 2009.

[21] Q. Wang, Y. Wang, Q. Meng et al., "Preparation of high antistatic HDPE/polyaniline encapsulated graphene nanoplatelet composites by solution blending," *RSC Advances*, vol. 7, no. 5, pp. 2796–2803, 2017.

[22] M. Rahaman, T. K. Chaki, and D. Khastgir, "Development of high performance EMI shielding material from EVA, NBR, and their blends: effect of carbon black structure," *Journal of Materials Science*, vol. 46, no. 11, pp. 3989–3999, 2011.

[23] Z. Jan and J. Maciej, "EMI shielding using composite materials with plasma layers," *Electromagnetic Waves*, vol. 425, 2011.

[24] J.-M. Thomassin, C. Jerome, T. Pardoen, C. Bailly, I. Huynen, and C. Detrembleur, "Polymer/carbon based composites as electromagnetic interference (EMI) shielding materials," *Materials Science and Engineering: R: Reports*, vol. 74, no. 7, pp. 211–232, 2013.

[25] D. Jiang, V. Murugadoss, Y. Wang et al., "Electromagnetic interference shielding polymers and nanocomposites-a review," *Polymer Reviews*, vol. 59, no. 2, pp. 280–337, 2019.

[26] R. Rohini and S. Bose, "Electromagnetic wave suppressors derived from crosslinked polymer composites containing functional particles: potential and key challenges," *Nano-Structures & Nano-Objects*, vol. 12, pp. 130–146, 2017.

[27] I. Arief, S. Biswas, and S. Bose, "Graphene analogues as emerging materials for screening electromagnetic radiations," *Nano-Structures & Nano-Objects*, vol. 11, pp. 94–101, 2017.

[28] L.-C. Jia, D.-X. Yan, C.-H. Cui, X. Jiang, X. Ji, and Z.-M. Li, "Electrically conductive and electromagnetic interference shielding of polyethylene composites with devisable carbon nanotube networks," *Journal of Materials Chemistry C*, vol. 3, no. 36, pp. 9369–9378, 2015.

[29] M. Rahaman, A. Aldalbahi, and P. Bhagabati, "Preparation/-processing of polymer–carbon composites by different techniques," in *Carbon-Containing Polymer Composites*, pp. 99–124, Springer, 2019.

[30] M. J. Cran, S. W. Bigger, and J. Scheirs, "Characterizing blends of linear low-density and low-density polyethylene by DSC," *Journal of Thermal Analysis and Calorimetry*, vol. 81, no. 2, pp. 321–327, 2005.

[31] J. Charles and G. R. Ramkumaar, "Qualitative analysis of high density polyethylene using FTIR spectroscopy," *Asian Journal of Chemistry*, vol. 21, no. 6, article 4477, 2009.

[32] J. V. Gulmine, P. R. Janissek, H. M. Heise, and L. Akcelrud, "Polyethylene characterization by FTIR," *Polymer Testing*, vol. 21, no. 5, pp. 557–563, 2002.

[33] A. Prasad, "A quantitative analysis of low density polyethylene and linear low density polyethylene blends by differential scanning calorimetery and fourier transform infrared spectroscopy methods," *Polymer Engineering & Science*, vol. 38, no. 10, pp. 1716–1728, 1998.

[34] M. S. Sh, F. G. Fard, E. Khatibi, and H. Sarpoolaky, "Dispersion and stability of carbon black nanoparticles, studied by ultraviolet-visible spectroscopy," *Journal of the Taiwan Institute of Chemical Engineers*, vol. 40, no. 5, pp. 524–527, 2009.

[35] P. Garg, B. P. Singh, G. Kumar et al., "Effect of dispersion conditions on the mechanical properties of multi-walled carbon nanotubes based epoxy resin composites," *Journal of Polymer Research*, vol. 18, no. 6, pp. 1397–1407, 2011.

[36] M. Rahaman, A. Aldalbahi, L. Nayak, and R. Giri, "Electrical conductivity of polymer–carbon composites: effects of different factors," in *Carbon-Containing Polymer Composites*, pp. 159–210, Springer, 2019.

[37] R. Ram, M. Rahaman, A. Aldalbahi, and D. Khastgir, "Determination of percolation threshold and electrical conductivity of polyvinylidene fluoride (PVDF)/short carbon fiber (SCF) composites: effect of SCF aspect ratio," *Polymer International*, vol. 66, no. 4, pp. 573–582, 2017.

[38] R. Ram, D. Khastgir, and M. Rahaman, "Electromagnetic interference shielding effectiveness and skin depth of poly(vinylidene fluoride)/particulate nano-carbon filler composites: prediction of electrical conductivity and percolation threshold," *Polymer International*, vol. 68, no. 6, pp. 1194–1203, 2019.

[39] M. Rahaman, T. K. Chaki, and D. Khastgir, "Determination of percolation limits of conductivity, dielectric constant, and EMI SE for conducting polymer composites using sigmoidal Boltzmann model," *Advanced Science Letters*, vol. 10, no. 1, pp. 115–117, 2012.

[40] M. Rahaman, A. Aldalbahi, P. Govindasami et al., "A new insight in determining the percolation threshold of electrical conductivity for extrinsically conducting polymer composites through different sigmoidal models," *Polymers*, vol. 9, no. 12, p. 527, 2017.

[41] M. E. Leyva, G. M. O. Barra, A. C. F. Moreira, B. G. Soares, and D. Khastgir, "Electric, dielectric, and dynamic mechanical behavior of carbon black/styrene-butadiene-styrene composites," *Journal of Polymer Science Part B: Polymer Physics*, vol. 41, no. 23, pp. 2983–2997, 2003.

[42] M. Rahaman, T. K. Chaki, and D. Khastgir, "Modeling of DC conductivity for ethylene vinyl acetate (EVA)/polyaniline conductive composites prepared through insitu polymerization of aniline in EVA matrix," *Composites Science and Technology*, vol. 72, no. 13, pp. 1575–1580, 2012.

[43] M. Rahaman, S. P. Thomas, I. A. Hussein, and S. K. De, "Dependence of electrical properties of polyethylene nanocomposites on aspect ratio of carbon nanotubes," *Polymer Composites*, vol. 34, no. 4, pp. 494–499, 2013.

[44] M. Rahaman, T. K. Chaki, and D. Khastgir, "Consideration of interface polarization in the modeling of dielectric property for ethylene vinyl acetate (EVA)/polyaniline conductive composites prepared through in-situ polymerization of aniline in EVA matrix," *European Polymer Journal*, vol. 48, no. 7, pp. 1241–1248, 2012.

[45] O. A. Bin-Dahman, M. Rahaman, D. Khastgir, and M. A. Al-Harthi, "Electrical and dielectric properties of poly (vinyl alcohol)/starch/graphene nanocomposites," *The Canadian Journal of Chemical Engineering*, vol. 96, no. 4, pp. 903–911, 2018.

[46] M. Rahaman, T. K. Chaki, and D. Khastgir, "High-performance EMI shielding materials based on short carbon fiber-filled ethylene vinyl acetate copolymer, acrylonitrile butadiene copolymer, and their blends," *Polymer Composites*, vol. 32, no. 11, pp. 1790–1805, 2011.

[47] Y. Sakaki and S. Imagi, "Relationship among eddy current loss, frequency, maximum flux density and a new parameter concerning the number of domain walls in polycrystalline and amorphous soft magnetic materials," *IEEE Transactions on Magnetics*, vol. 17, no. 4, pp. 1478–1480, 1981.

[48] S. T. Sam, H. Ismail, M. N. A. Fauzi, and A. A. Bakar, "The effect of carbon black on the properties of magnetic ferrite filled natural rubber composites," *Journal of Reinforced Plastics and Composites*, vol. 27, no. 16-17, pp. 1893–1908, 2008.

[49] M. Rahaman, I. A. Hussein, A. Aldalbahi, A. Parvez, and J. B. P. Soares, "Synthesis of metallocene catalyzed ethylene 1, 7-octadiene copolymer: effect of copolymerization on

polymer properties," *Macromolecular Research*, vol. 26, no. 4, pp. 295–304, 2018.

[50] L. G. Barbosa, M. Piaia, and G. H. Ceni, "Analysis of impact and tensile properties of recycled polypropylene," *International Journal of Materials Engineering*, vol. 7, no. 6, pp. 117–120, 2017.

[51] J. Z. Liang and Q. Q. Yang, "Mechanical properties of carbon black-filled high-density polyethylene antistatic composites," *Journal of Reinforced Plastics and Composites*, vol. 28, no. 3, pp. 295–304, 2008.

[52] K. Sasikumar, N. Manoj, T. Mukundan, M. Rahaman, and D. Khastgir, "Mechanical properties of carbon-containing polymer composites," in *Carbon-Containing Polymer Composites*, pp. 125–157, Springer, 2019.

[53] I. Chodak and I. Krupa, ""Percolation effect" and mechanical behavior of carbon black filled polyethylene," *Journal of Materials Science Letters*, vol. 18, no. 18, pp. 1457–1459, 1999.

[54] L. Nayak, M. Rahaman, D. Khastgir, and T. K. Chaki, "Thermal degradation kinetics of polyimide nanocomposites from different carbon nanofillers: applicability of different theoretical models," *Journal of Applied Polymer Science*, vol. 135, no. 7, article 45862, 2018.

[55] R. Ram, M. Rahaman, and D. Khastgir, "Electromagnetic interference (EMI) shielding effectiveness (SE) of polymer-carbon composites," in *Carbon-Containing Polymer Composites*, pp. 339–368, Springer, 2019.

[56] M. Rahaman, L. Nayak, T. K. Chaki, and D. Khastgir, "Conductive composites made from <I>In-Situ</I> polymerized polyaniline in ethylene vinyl acetate copolymer (EVA): mechanical properties and electromagnetic interference shielding effectiveness," *Advanced Science Letters*, vol. 18, no. 1, pp. 54–61, 2012.

[57] N. F. Colaneri and L. W. Schacklette, "EMI shielding measurements of conductive polymer blends," *IEEE Transactions on Instrumentation and Measurement*, vol. 41, no. 2, pp. 291–297, 1992.

[58] Y.-J. Yim and S.-J. Park, "Electromagnetic interference shielding effectiveness of high-density polyethylene composites reinforced with multi-walled carbon nanotubes," *Journal of Industrial and Engineering Chemistry*, vol. 21, pp. 155–157, 2015.

[59] B. P. Singh, Prabha, P. Saini et al., "Designing of multiwalled carbon nanotubes reinforced low density polyethylene nanocomposites for suppression of electromagnetic radiation," *Journal of Nanoparticle Research*, vol. 13, no. 12, pp. 7065–7074, 2011.

[60] M. H. Al-Saleh and U. Sundararaj, "Electromagnetic interference shielding mechanisms of CNT/polymer composites," *Carbon*, vol. 47, no. 7, pp. 1738–1746, 2009.

[61] T. K. Gupta, B. P. Singh, S. R. Dhakate, V. N. Singh, and R. B. Mathur, "Improved nanoindentation and microwave shielding properties of modified MWCNT reinforced polyurethane composites," *Journal of Materials Chemistry A*, vol. 1, no. 32, pp. 9138–9149, 2013.

[62] S. Pande, B. P. Singh, R. B. Mathur, T. L. Dhami, P. Saini, and S. K. Dhawan, "Improved electromagnetic interference shielding properties of MWCNT–PMMA composites using layered structures," *Nanoscale Research Letters*, vol. 4, no. 4, pp. 327–334, 2009.

[63] C. Li, G. Yang, H. Deng et al., "The preparation and properties of polystyrene/functionalized graphene nanocomposite foams using supercritical carbon dioxide," *Polymer International*, vol. 62, no. 7, pp. 1077–1084, 2012.

[64] N. Agnihotri, K. Chakrabarti, and A. De, "Highly efficient electromagnetic interference shielding using graphite nanoplatelet/-poly (3, 4-ethylenedioxythiophene)–poly (styrenesulfonate) composites with enhanced thermal conductivity," *RSC Advances*, vol. 5, no. 54, pp. 43765–43771, 2015.

[65] A. A. Kareem, "Preparation and electrical properties of polyimide/carbon nanotubes composites," *Materials Science-Poland*, vol. 35, no. 4, pp. 755–759, 2018.